


Post-failure topographical assessment of carbon fiber reinforced polymer – reinforced S235R steel under tensile loading

Aleksandra Mirowska^{1,2}, Wojciech Macek^{1,2*} ,
Wiktoria Wojnicz¹, Grzegorz Gajowiec¹, Maciej Kowal³

¹ Faculty of Mechanical Engineering and Ship Technology, Gdansk University of Technology,
Gabriela Narutowicza 11/12, 80-233 Gdansk, Poland

² Advanced Materials Center, Gdansk University of Technology, Gabriela Narutowicza 11/12, 80-233 Gdansk,
Poland

³ Faculty of Civil Engineering and Architecture, Lublin University of Technology, Nadbystrzycka 40, 20-618
Lublin, Poland

* Corresponding author's e-mail: wojciech.macek@pg.edu.pl

ABSTRACT

The application of the adhesive-bonded CFRP laminates prolonged the durability of steel specimens. This study investigated the influence of carbon fiber reinforced polymer (CFRP) tape reinforcement on the fracture surface characteristics of S235JR carbon steel specimens subjected to uniaxial static tensile load. The steel specimens were reinforced with high strength unidirectional CFRP plates, while one unreinforced specimen served as a reference. To evaluate the topographical and morphological features of all fracture surfaces the 3D optical profilometry and scanning electron microscopy had been used. The chosen ISO 25178-compliant roughness parameters were calculated, including height, functional, and functional volume parameters, as well as non-standard descriptors, such as furrow geometry and texture isotropy. The results indicate that height parameters are not significantly affected by the presence of CFRP, since they are sensitive to localized anomalies. In contrast, the functional and functional volume parameters revealed notable differences: reinforced specimens showed lower values of peak material volume V_{mp} and core void volume V_{vc} along with reduced plastic deformation and more localized fracture behavior. Additionally, peak material portion S_{mr1} and valley material portion S_{mr2} were slightly higher in the unreinforced specimen, indicating more homogeneous plastic deformation. Analysis of furrow geometry and texture isotropy revealed that unreinforced steel exhibited ductile fracture with high furrow density and isotropic texture, while CFRP reinforcement introduced anisotropy texture and features associated with mixed ductile-brittle fracture. The presented findings demonstrate the significant impact of composite on fracture mechanisms and surface morphology of the reinforced specimens.

Keywords: entire fracture surface, quantitative fractography, surface topography, S235R steel, CFRP.

INTRODUCTION

The mechanical performance and structural reliability of metallic components subjected to service loads have long been critical concerns in the engineering domain, particularly in the applications involving civil infrastructure, transportation systems, and heavy machinery [1]. Among the commonly used structural steels, S235R has established itself as a material of choice due to

its optimum combination of ductility, weldability, and strength by making it particularly suitable for load-bearing applications [2]. However, under tensile loading and long-term operational stress, metallic structures often suffer from various forms of degradation, including fatigue, corrosion, and mechanical failure. This has necessitated the exploration of advanced reinforcement techniques aimed at prolonging structural life and enhancing mechanical performance [3].

One promising feasibility in recent decades has been the application of composites containing fiber-reinforced polymer (FRP) used as external reinforcements to existing metallic or concrete elements. Among these, carbon fiber-reinforced polymers (CFRPs) have garnered considerable interest due to their exceptional specific strength, stiffness, and resistance to environmental degradation [4]. The integration of conventional ductile metals, like steel with advanced carbon fiber-reinforced polymer composites, engenders a synergistic interaction that significantly broadens the scope for innovative approaches in structural rehabilitation and the engineering of hybrid material systems. In particular, reinforcing steel substrates with CFRP laminates can significantly improve load-bearing capacity and delay the onset of critical failure modes, such as yielding or brittle fracture. Mohabeddine et al. [5] present the prediction of fatigue life of metallic structural details reinforced with CFRP. The authors introduced the cycle-dependent stiffness degradation parameter of the composite patch. Duda et al. [6] analyzed the mechanical performance of CFRP thin-walled structures under multiaxial loadings. Their nonlinear shear model, based on the FEA, showed a good agreement for damage distribution with the experiment.

Despite numerous studies that have quantified the mechanical enhancements afforded by CFRP reinforcement, less attention has been directed towards a comprehensive understanding of the post-failure morphology of these hybrid systems [7]. The fracture topography provides the information regarding the failure mechanisms, energy dissipation characteristics, and the role of microstructural features in crack propagation [8]. Fractographic analysis, especially when performed in a quantitative manner using surface topography parameters, enables the detailed examination of the interplay between reinforcement and matrix material during failure [9–11]. Such analyses are particularly relevant in hybrid steel-composite systems, where complex interactions at the interface between steel and CFRP layers can result in non-trivial stress redistributions and fracture pathways.

Analysis of surfaces of materials – both prior to use and after failure – provides valuable insights into their durability and load-bearing capabilities [12, 13]. Fractography, in particular, which involves the analysis of fracture surfaces, can reveal important details about the history of the material, leading up to its failure [14, 15]. External factors,

such as elevated temperatures, are often reflected in the fracture topography [16, 17]. Advanced measurement techniques, including digital image correlation and various forms of microscopy [18, 19], are especially useful for quantitative fracture surface analysis. Combining modern research methods with optical surface observation techniques also enables the development of alternative approaches to fracture surface characterization, such as the FRASTA (fracture surface topography analysis) method [20, 21] or the Entire Fracture Surface Topography method [22, 23]. These measurement tools further support the refinement of classical computational models and the exploration of unconventional approaches, such as fractal dimension analysis [24, 25].

This study aimed to bridge this gap by conducting an exhaustive topographical investigation of the fracture surfaces of S235R steel specimens reinforced with CFRP composites and subjected to uniaxial static tensile testing. In the scope of this study post-mortem surfaces are characterized by assessing the parameters of surface metrology along with statistical parameters (roughness, skewness, kurtosis, and fractal dimension) [26–28]. The obtained results are used to reveal the underlying failure mechanisms and to distinguish between ductile and brittle failure modes, to identify the areas of localized stress concentration, and to assess the influence of reinforcement on crack initiation and propagation [29].

METHODOLOGY

In this study, the authors tested the specimens produced from S235JR carbon steel. The chemical composition of the steel is provided in Table 1.

As the first step of the experiments, the mechanical properties of the steel plates were determined through tensile coupon tests at ambient temperature. Considering the results of these tests, the following mechanical properties were assessed: Young modulus of 205 GPa, yield strength of 287.1 MPa, ultimate tensile strength of 432.0 MPa, and ultimate tensile elongation 0.25%.

To produce CFRP reinforced specimens, high modulus unidirectional plates were used as the patching system. The composite S&P CFK-Lamellen 200/2000 tapes based on epoxy resins with carbon fibers were selected as reinforcement. The width of the tapes was 20 mm and a thickness of 1.4 mm. According

Table 1. Chemical composition (wt%) of S235JR steel specimens tested in the study

Parameter	Fe	C	Mn	P	S	N	Cu
Wt%	balance	≤ 0.17	≤ 1.40	≤ 0.035	≤ 0.035	≤ 0.12	≤ 0.55

to the manufacturer, the mechanical properties of CFRP plate are following: ultimate tensile strength of 2500 MPa, ultimate strain of 1.25% and Young modulus of 210.0 GPa.

Eight specimens were reinforced by CFRP tapes of 300 mm long and 20 mm wide, bonded at distance of 8 mm from the edge of the hole taking into account the presence of the rivet head. The geometry of the reinforced specimens is presented in Figure 1. The configuration of the tape arrangement and end shapes is presented in Table 2. Also, a reference specimen was prepared as one with no reinforcement tapes (unreinforced specimen).

Uniaxial static tensile tests of a reference steel specimen and eight composite-reinforced specimens were performed on the MTS 809 Axial/Torsional testing machine (model No 319.2) with load range 250 kN. All tests were performed by controlling a displacement of the piston equaled 0.45 mm/min.

In this study, the observations of the fracture surfaces were performed on both sides of the specimens, which has accumulated to a total of

18 entire fracture surfaces studied. The entire fracture area measurements were performed by using the Sensofar S neox 090 3D optical profilometer utilizing confocal microscopy technique. These measurements were conducted by using the Nikon EPI objective with a 5.0× magnification. The pixel size was 2.76 $\mu\text{m}/\text{pixel}$. The SensoSCAN S neox 7.7 software was applied to collect the fracture surface images. The data files were transferred to the surface texture analysis software MountainsMap 8.0 and resampled into height maps. Chosen ISO 25178 surface topography parameters were calculated and analyzed [30, 31]:

- Height parameters: arithmetical mean height (S_a), root mean square height (S_q), maximum height (S_z), maximum peak height (S_p), maximum pit height (S_v), skewness (S_{sk}), kurtosis (S_{ku});
- Functional parameters: core roughness depth (S_k), reduced peak height (S_{pk}), reduced dale height (S_{vk}), peak material portion (areal material ratio dividing the reduced peaks from the core surface) (S_{mr1}), valley material portion

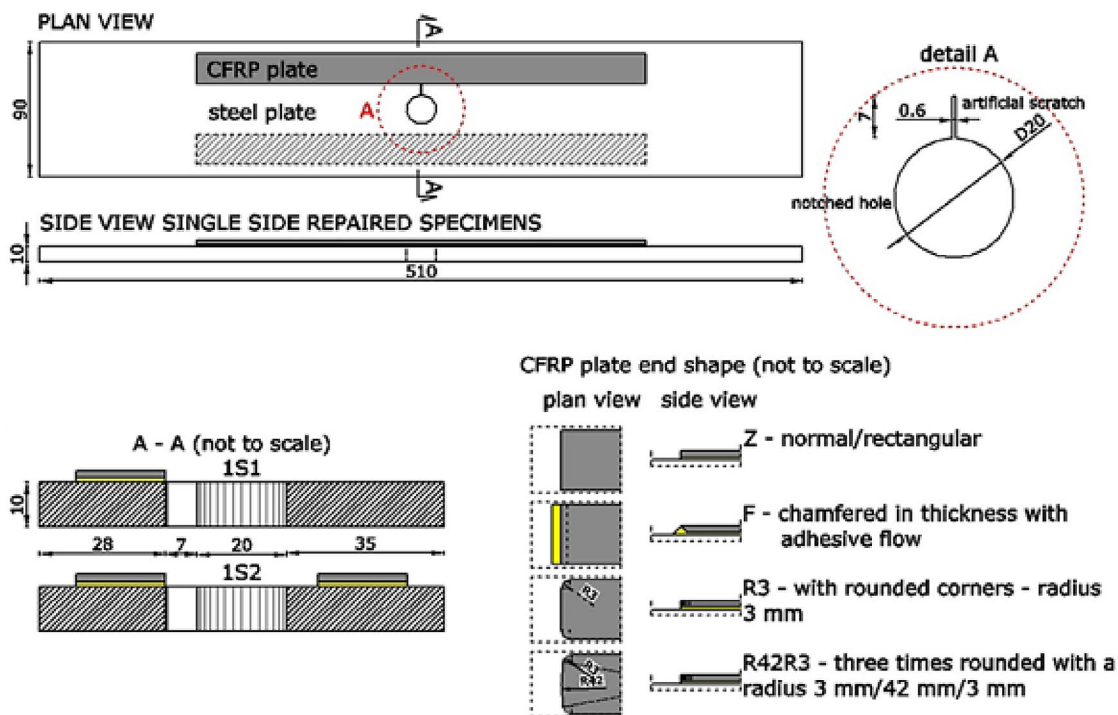


Figure 1. Geometry of the reinforced specimens prepared for the tensile testing

Table 2. Tape arrangement and end shape of the produced specimens

Specimen designation	Tape arrangement	CFRP tape end shape
Ref	-	-
1S1-Z	Single side of the specimen, one tape	Rectangular
1S2-Z	Single side of the specimen, two tapes	Rectangular
1S1-F	Single side of the specimen, one tape	Chamfered in thickness with adhesive flow
1S2-F	Single side of the specimen, two tapes	Chamfered in thickness with adhesive flow
1S1-R3	Single side of the specimen, one tape	With rounded corners – radius of 3 mm
1S2-R3	Single side of the specimen, two tapes	With rounded corners – radius of 3 mm
1S1- R42R3	Single side of the specimen, one tape	Three times rounded with a radius 3 mm/ 42 mm/ 3 mm
1S2- R42R3	Single side of the specimen, two tapes	Three times rounded with a radius 3 mm/ 42 mm/ 3 mm

(areal material ratio dividing the reduced valleys from the core surface) (Smr2);

- Functional volume parameters: material volume (Vm), void volume (Vv), peak material volume (Vmp), core material volume (Vmc), core void volume (Vvc), valley void volume (Vvv).

Texture isotropy and non-standard parameters, such as maximum depth of furrows and mean density of furrows were also calculated using mentioned software, without applying any additional filtering.

The fracture surfaces of all tested samples were inspected with a high resolution scanning electron microscope Tescan Vega along with a secondary electron detector operating at an acceleration voltage of 15 keV.

RESULTS AND DISCUSSION

To obtain an analyzed 3D fracture surface topography of each tested fracture, an inspected surface was modified by filling non-measured points (NMPs) through an interpolation method. Next, the region of interest (ROI) was exported from this updated surface. The study area was limited to a rectangle measuring 24 mm by 7 mm. This ROI has the same area for all tested specimens. Figure 2 presents the observed surface (see Figure 2(a) and 2(b)) and its extraction for ROI (see Figure 2(c) and 2(d)).

The standardized surface roughness height parameters *S* are frequently employed to quantitatively characterize the topography of fracture surfaces in metallic materials [32, 33]. These parameters reflect the geometric features of the surface and serve as reliable indicators of its structural

condition and quality. In the context of fracture analysis, these indicators facilitate a deeper understanding of the dominant fracture mechanisms and to establish the main conditions that governed the failure process [34–36]. Figure 3 presents bar charts of the seven height parameters assessed for two fractures of each tested specimen.

The parameters *Sa*, *Sq*, *Sz*, *Sp*, and *Sv* (*Sx*) represent general amplitude characteristics of the surface. These parameters are sensitive to local variations; however, they do not specifically capture the directionality or functional distribution of surface features. In both reinforced and reference specimens, despite differences in fracture mechanisms, the overall surface roughness amplitude can remain similar due to compensating effects. Ductile fractures produce more uniform but widespread deformation, while brittle fractures result in localized sharper features, which may average out to comparable values in terms of *Sx* parameters. Therefore, these parameters do not clearly differentiate the influence of CFRP reinforcement, as they lack a sensitivity to fracture mode or anisotropy due to focusing only on overall surface height variations. On the other hand, the *Ssk* parameter measures the asymmetry of the height distribution and it can take positive or negative values, but even small local peaks or valleys can significantly affect its value. Both brittle and ductile fractures can have different local forms and this leads to a lack of a clear trend. The *Sku* parameter can be strongly affected by single extreme points, regardless of the fracture mechanism. Moreover, differences between samples may be more caused by the random nature of the fractures than the presence or absence of reinforcement.

Functional parameters such as *Sk*, *Spk*, *Svk*, *Smr1* and *Smr2* provide detailed information about the distribution of surface profile heights

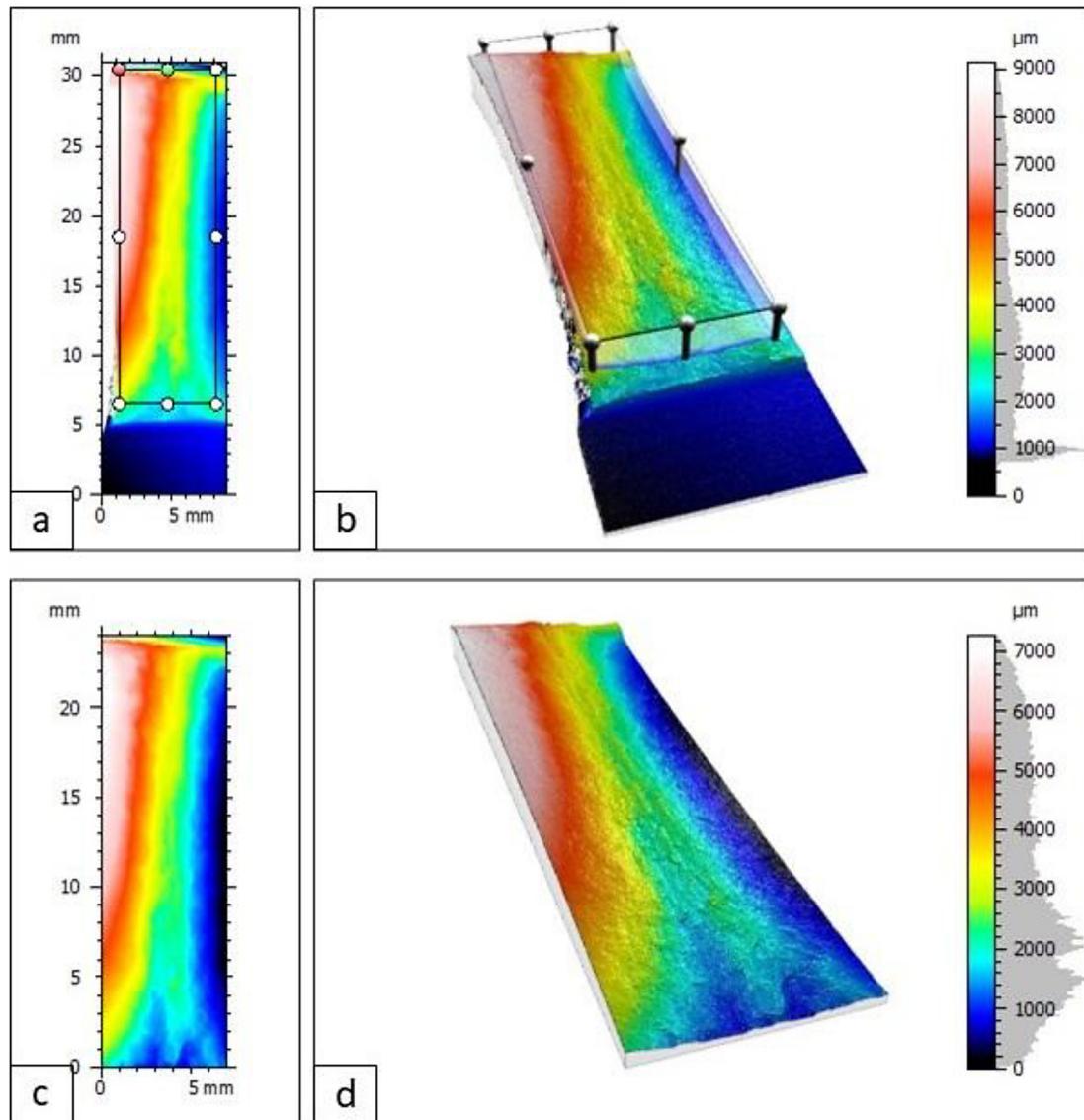


Figure 2. Contour maps present: 2D picture (a) and 3D picture (b) of inspected surfaces with filled NMPs and indication of ROI; 2D picture (c) and 3D picture (d) with the extracted ROI surface

referring to bearing capacity, deformation and damage. Figure 4 presents the values of functional parameters for all fractures of eight specimens tested in this study.

The S_k parameter shows no clear trend, because it reflects the core roughness, which depends on a complex interplay of surface features influenced by both material deformation and fracture mode. In reinforced samples, local stress concentrations and anisotropic constraints can either increase or decrease core roughness compared to the unreinforced sample, leading to inconsistent variations without a systematic dependence. No significant differences in the S_{pk} parameter were observed in the case of the reference and reinforced samples. When inspecting

a reference sample, one can notice that plastic deformation creates numerous small-scale peaks due to microvoid coalescence and tearing, but these peaks tend to be relatively rounded and less sharp. Meanwhile, when inspecting the reinforced specimens, one can identify that a brittle character of the fracture produces sharper and more pronounced peaks, and these features may be fewer in number and more localized. As a result, the overall height of the reduced peaks averages out to similar values across both types of fractures, reflecting a balance between many small rounded peaks in ductile fractures and fewer but sharper peaks in brittle fractures. The S_{vk} parameter, which represents the reduced valley depth, was lower for the unreinforced material compared to

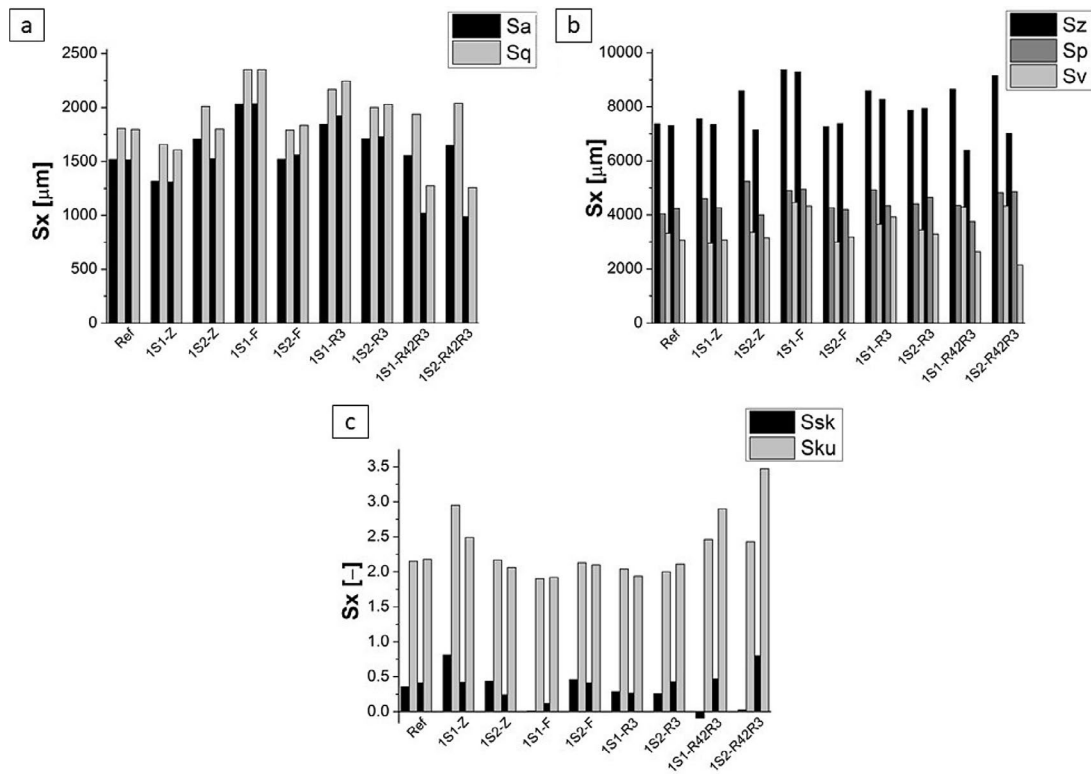


Figure 3. Bar graphs of height parameters – Sa and Sq (a), Sz, Sp and Sv (b), Ssk and Sku (c) for all tested specimens

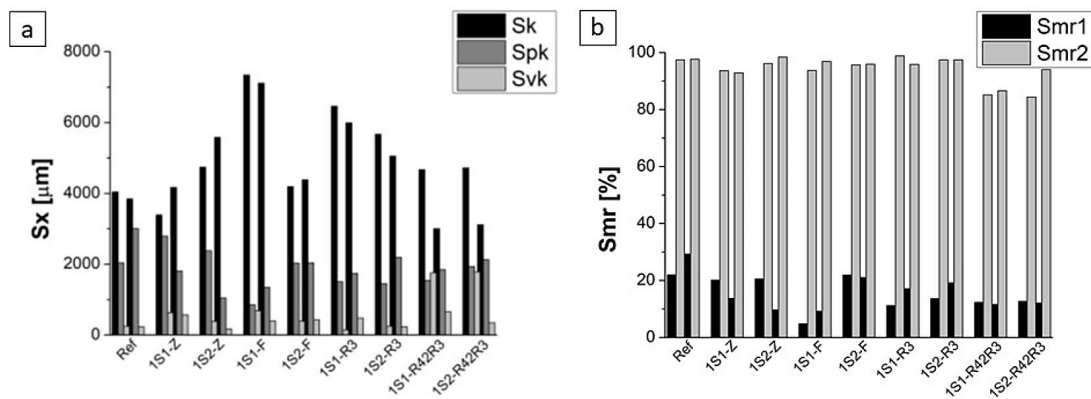


Figure 4. Bar graphs of functional parameters – Sk, Spk and Skv (a), Smr1 and Smr2 (b) for all tested specimens

the reinforced specimens due to differences in fracture mechanisms and surface morphology. When inspecting an unreinforced specimen, one can identify that fracture occurs through extensive plastic deformation that leads to a more uniform and rounded surface with shallower valleys, as a result of ductile fracture. This results also in fewer deep cracks or cavities (lower Sv_k values). In contrast, the CFRP-reinforced specimens tend to exhibit more brittle or mixed-mode fracture behavior, characterized by sudden crack propagation and localized material separation. This

produces sharper and deeper valleys on the fracture surface, increasing the Sv_k parameter. The reinforcement constrains deformation and promotes anisotropic crack paths, which contribute to the formation of pronounced valleys and higher Sv_k values. The slightly higher values of Smr1 and Smr2 observed in the unreinforced specimen can be explained by the nature of its fracture surface and involved ductile failure mechanism. In a ductile fracture of the reference sample, one can identify that the material undergoes significant plastic deformation before rupture. This results

in a more uniform and smoother surface profile, with fewer extreme peaks or valleys, and a more evenly distributed material height. As a result, the percentage of the surface area located above the core and below the core is slightly higher because the height distribution is broader but less extreme, which can be explained by higher values of Smr1 and Smr2 parameters. In contrast, the reinforced specimens due to more brittle or mixed-mode fracture mechanisms develop surfaces with sharper peaks and deeper valleys that are often localized. These features increase the kurtosis (Sku) and create a more extreme surface profile, but reduce the relative amount of surface area close to the core height, thereby lowering Smr1 and Smr2.

According to ISO 25178, the functional volume parameters play a key role in the analysis of fracture surfaces by giving in-depth information on surface morphology and fracture features [37]. Figure 5 presents a summary of the measured values of these parameters for two fractures of each specimen.

The slight increase in the values of the Vm, Vmc and Vvv parameters for the reinforced specimens compared to the unreinforced specimens is due to the influence of the more brittle and locally violent nature of fracture, which is typical of materials with CFRP reinforcement. The value of the Vmc parameter is increased for reinforced specimens compared to unreinforced steel. The reason of this are brittle fractures due to the influence of added reinforcement that generates steeper and sharper structures on the surface that increase the volumes counted in 3D analysis, even though they are more local. In the case of the Vvv parameter, a gentle increase was also observed, as deeper and more abrupt valleys are typical

of brittle fractures – fracture occurs quickly and with less extension, leading to deeper voids and micro-cracks. The Vmp parameter is decreased in reinforced specimens, because CFRP reinforcement limits plastic deformation and promotes more brittle fracture mechanisms, in which multiple protrusions and stretches of material are not formed at the fracture surface. In the case of the reference sample, the ductile fracture results in a formation of numerous but mild elevations on the surface, like through micro-cracks, merging of micro-cavities, local outflows of material, and this results in a larger volume of material above the core. In contrast, reinforced specimens manifest cracking more violently and without stretching, have a surface with fewer peaks and heights, resulting in a lower Vmp. When analyzing the Vvc parameter, it is observed that its value decreases for unreinforced samples. Although CFRP reinforcement promotes more brittle fracture, the local valleys are deeper but less extensive in surface area than in ductile fracture. In an unreinforced specimen, the material is stretched and plastic deformation results in more extensive microcavities and valleys below the core. Moreover, even if they are not very deep, they cover a larger area and increase the total volume Vvc. In reinforced samples, although the valleys may be steeper and point-deeper, the values of the Svk and Vvv parameters are increased and they are less numerous as well as have a smaller area by leading to a smaller total volume of voids below the core and a decrease in the value of the Vvc parameter.

Figure 6 presents a graphical depiction of functional volume and functional parameters for the reference specimen and a representative CFRP reinforced sample 1S1_R42R3.

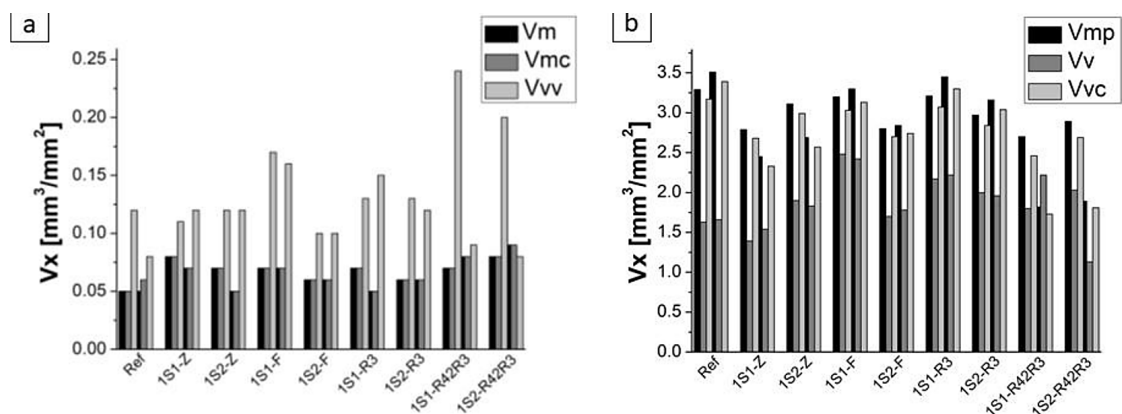


Figure 5. Bar graphs of functional volume parameters – Vm, Vmc and Vvv (a), Vmp, Vv and Vvc (b) for all tested specimens

In this study, the texture isotropy parameter referring to the fracture surface topography was assessed. The directional characteristics of the surface texture are shaped by crack propagation and are directly linked to the kinematics of the fracture process [38]. Moreover, an isotropic surface exhibits uniform physical and geometric properties in all directions. In the scope of the presented study, the texture isotropy was determined through the evaluation of the autocorrelation function that assesses the directional uniformity and potential periodicity of the surface. This parameter provides valuable insight into the anisotropy induced by the fracture mechanism. Figure 7 presents the texture isotropy for the reference sample and chosen representative CFRP specimen (1S1_R42R3).

According to the reported evidence, the reinforced specimens exhibited lower isotropy in comparison to unreinforced specimens. Higher isotropy observed on the fracture surface of the

unreinforced specimen can be attributed to the uniform stress distribution within the material during uniaxial static tensile loading. Without the presence of external reinforcements, the S235JR base material undergoes plastic deformation and eventual failure in a relatively homogeneous manner. The fracture propagates without a preferred orientation, resulting in a surface morphology that is more uniform and directionally nature. This leads to a higher degree of isotropy on the fracture surface. In contrast, the specimens reinforced with CFRP tapes exhibit a lower degree of isotropy. The addition of unidirectional CFRP tapes significantly alters the stress distribution within the specimen. Due to the high stiffness and strength of CFRP, as well as its directional nature, plastic deformation in the reinforced region is constrained. This introduces anisotropy in the mechanical response of the specimen, particularly near the CFRP-stiffened zones. As a result, crack initiation and propagation become

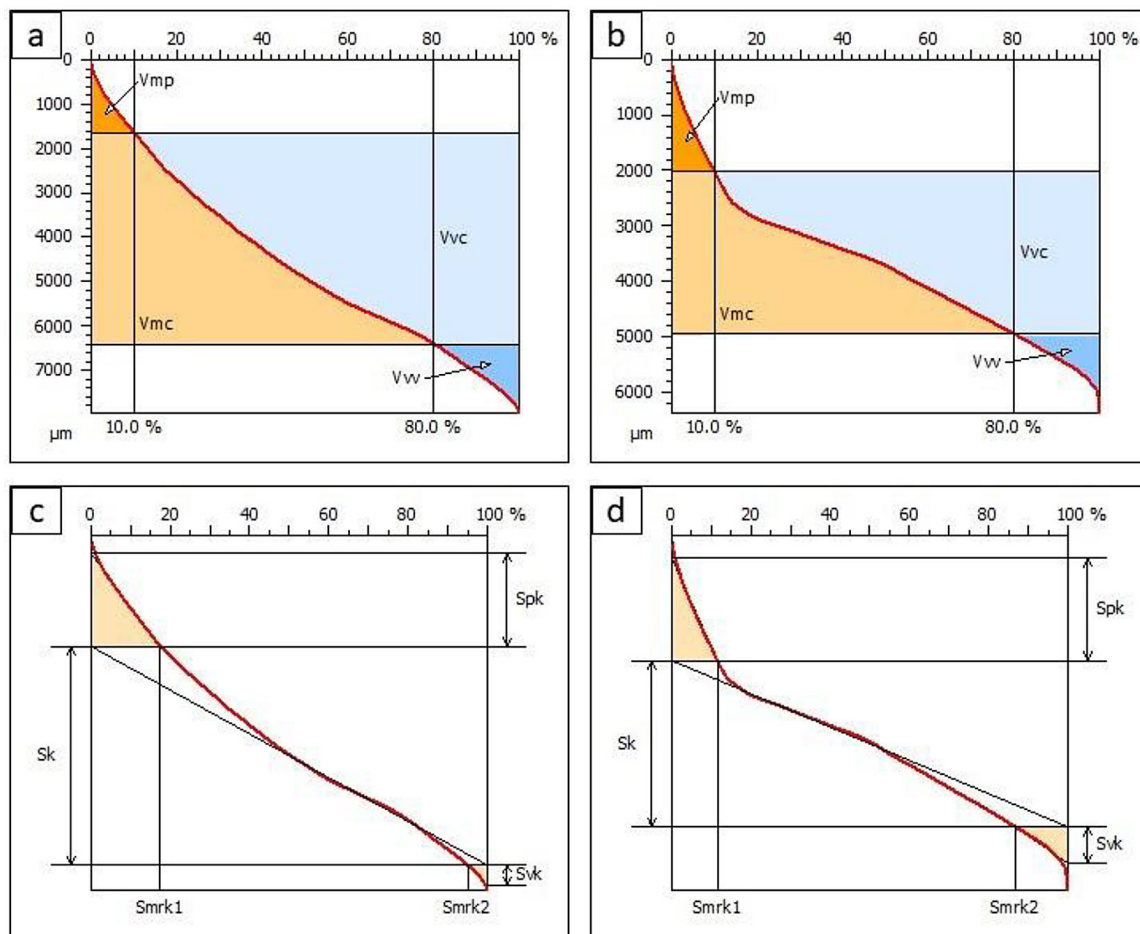


Figure 6. Graphical representation of discussed functional volume parameters (a and b) and functional parameters (c and d) for the unreinforced specimen (a and c) and representative CFRP reinforced specimen – 1S1_R42R3 (b and d)

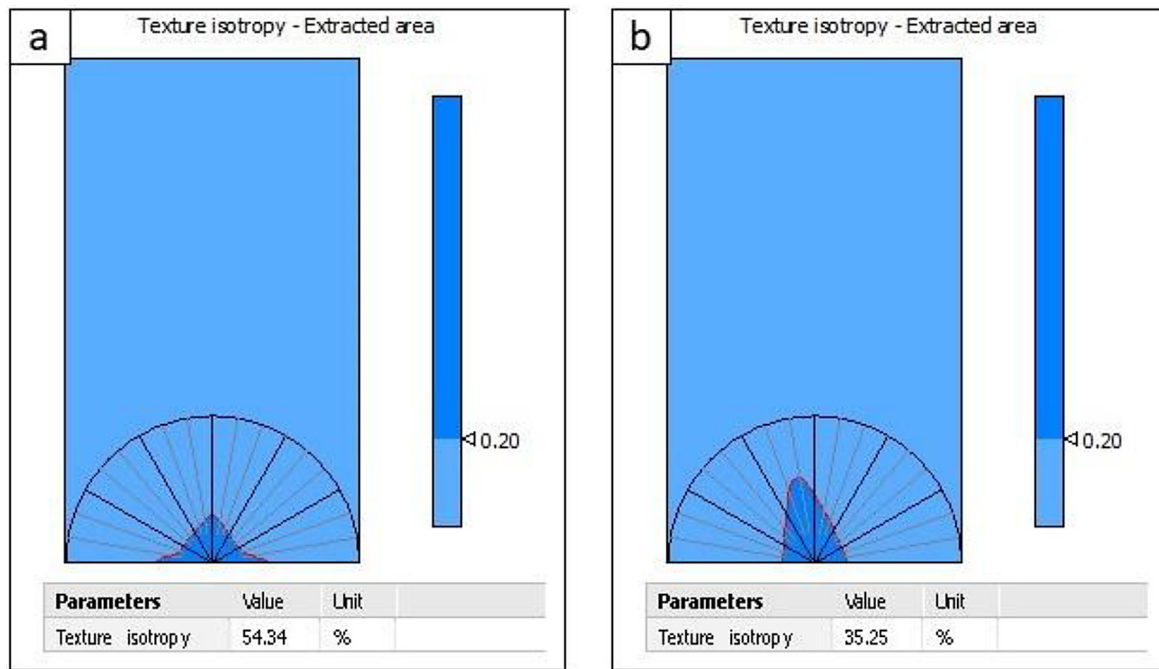


Figure 7. Texture isotropy of the unreinforced specimen and representative CFRP reinforced specimen – 1S1_R42R3

directionally influenced, often occurring along the interface between the steel and the composite or in the regions where stress concentrations are elevated due to the presence of the reinforcement. Consequently, the fracture surface becomes more directional and exhibits features characteristic of anisotropic failure.

The analysis of furrow depth (both maximum and mean) as well as furrow density is essential for characterizing fracture surfaces and for identification of the microstructural response of the material during crack propagation. Greater furrow depths typically indicate more brittle fracture behavior and is associated with sudden energy release along with localized material separation. On the other hand, higher furrow density suggests ductile behavior that involves extensive micro-cracking and plastic deformation. The described metrics provide valuable insight into the fracture mechanism and complement standard surface roughness parameters in evaluating failure characteristics. Figure 8 presents the graphical representation of furrow characteristics of the reference sample and chosen CFRP reinforced specimen, while Figure 9 shows the values of the maximum and mean depth of furrows (a) and mean density of furrows (b) for all the tested specimens.

The unreinforced specimen exhibited lower values of maximum depth of furrows and mean depth of furrows compared to some

CFRP-reinforced specimens, although all reinforced specimens simultaneously show a lower mean density of furrows with respect to the reference one. This can be explained by considering the differences in fracture mechanisms and surface morphology. In the unreinforced specimen, the material failed under relatively uniform tensile stress, leading to a more ductile fracture process with evenly distributed plastic deformation. As a result, the surface of the fracture showed a finer and more homogeneous topography. These furrows are shallower on average and lack deep localized features, leading to lower maximum and mean depth values. However, due to the uniformity of the ductile fracture mechanism, the surface is covered with a greater number of these small features and this causes a higher mean density of furrows. On the other hand, the presence of CFRP reinforcement alters the stress distribution and restricts plastic deformation in specific regions. The increased stiffness caused by the localized constraints (imposed by the CFRP) produce more concentrated and abrupt fracture paths, particularly in the areas near the interface between the composite and the steel substrate. This often leads to more brittle-like failure modes or mixed-mode fracture, which produce fewer but significantly deeper furrows due to sudden crack propagation and localized material separation. Consequently, the maximum and mean depth of

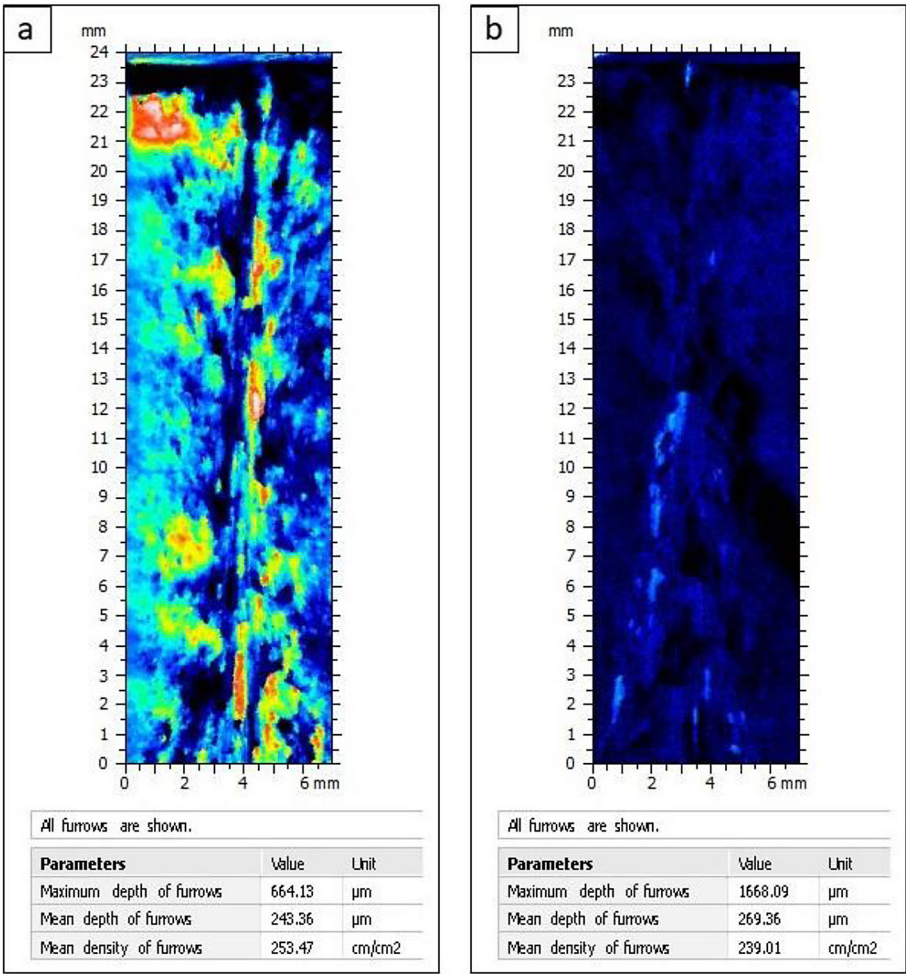


Figure 8. Graphical representation of furrows for extracted ROIs for the unreinforced specimen (a) and a representative CFRP reinforced specimen – 1S1_R42R3 (b)

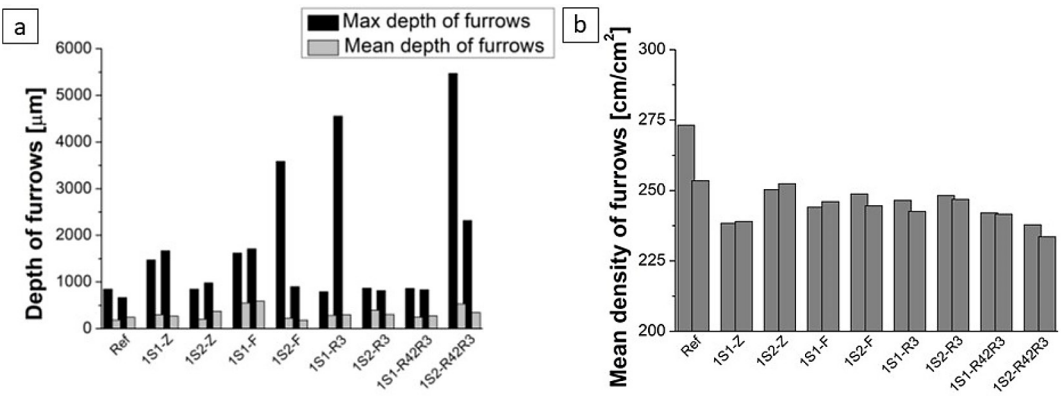


Figure 9. The values of the maximum and mean depth of furrows (a) and mean density of furrows (b) obtained for all the tested samples

furrows increase, while the overall number of furrows decreases, leading to a lower mean density.

The tested samples were also observed with the use of high-resolution scanning electron microscope. Figure 10 presents the fracture surfaces of the reference unreinforced specimen and

chosen sample with CFRP tape (1S1_R42R3). Both fractures exhibit features characteristic of ductile failure, such as visible dimples and evidence of plastic deformation. However, the surface of the CFRP-reinforced sample also shows localized brittle features – such as sharper edges

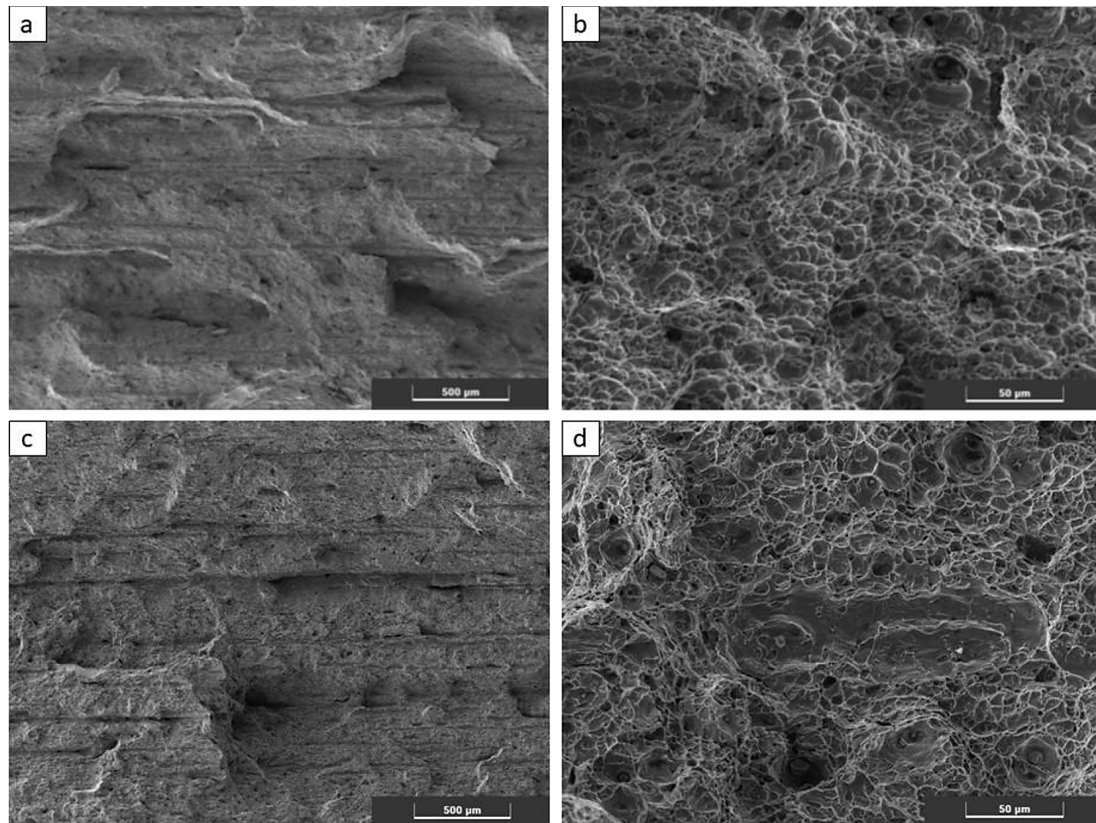


Figure 10. SEM pictures of the unreinforced specimen (a and b) and representative CFRP reinforced specimen – 1S1_R42R3 (c and d)

and cleavage-like regions – indicating a mixed fracture mode resulting from the constraint effects introduced by the composite reinforcement. These brittle features observed in the CFRP-reinforced specimen arise due to the constraint effect imposed by the high-stiffness composite material. The CFRP tape limits the local plastic deformation of the steel, especially near the fracture zone, which leads to stress concentration and reduced ductility in those regions. As a result, the material is more prone to localized brittle cracking, even though the overall fracture remains predominantly ductile. This mixed-mode failure is observed when a ductile substrate is reinforced with a much stiffer and less deformable material like CFRP.

CONCLUSIONS

Considering the presented results, following main conclusions were formulated:

1. Height parameters (S_a , S_q , S_z , S_p , S_v , S_{ku} and S_{sk}) do not show a clear influence of CFRP reinforcement, because these height parameters are sensitive to local anomalies and do not clearly

reflect the type of fracture and/or the influence of anisotropy introduced by the reinforcement.

2. The decrease in V_{mp} in the reinforced specimens is caused by a reduction of plastic strain and the formation of protrusions on the fracture surface. This behavior is induced by the presence of CFRP that caused more brittle nature of fracture. The decrease in V_{vc} in reinforced specimens is due to the more localized nature of the cracks. The valleys are deeper but less extensive and this reduces the total volume of voids relative to the more stretched ductile surface of unreinforced steel.
3. The unreinforced specimen exhibited slightly higher S_{mr1} and S_{mr2} values and also reflects more uniform distribution of surface heights resulting from ductile fracture and evenly distributed plastic deformation. In contrast, the reinforced specimens showed lower material ratios due to more localized and anisotropic fracture features caused by constrained crack propagation influenced by the CFRP reinforcement.
4. The analysis of furrow geometry and surface isotropy leads to consistent and mutually reinforcing conclusions about the fracture

behavior of the tested specimens. In the unreinforced specimen, the fracture process was governed by relatively uniform stress distribution and unrestricted plastic deformation that led to a ductile fracture mechanism (a high density of shallow furrows formed in various directions without a dominant orientation) that has an isotropic texture. Due to the directional stiffness influenced by CFRP tape (tapes) the reinforcement introduced significant anisotropy in the mechanical response and the fracture surface exhibited deeper furrows with lower density.

5. The analysis of furrows and surface isotropy leads to consistent conclusions about fracture behavior. In the unreinforced specimen, uniform stress distribution caused ductile isotropic failure with many shallow and randomly oriented furrows indicating high isotropy. In contrast, the CFRP-reinforced specimens showed deeper but fewer furrows, aligned with the reinforcement direction that reflect anisotropic crack propagation. Moreover, furrow geometry and isotropy measurements confirm that reinforcement introduces directional constraints that caused less uniform and more anisotropic fracture.
6. In light of increasing demands for lightweight, durable, and retrofitable engineering solutions, understanding the fracture behavior of such hybrid materials is both timely and technically significant. The results of this study have practical implications for the design of reinforced steel structures, predictive modeling of failure, and the development of advanced composite-steel hybrid systems. Furthermore, the research aligns with current trends in sustainable engineering by enabling the extension of service life in existing structures through non-invasive reinforcement techniques.
7. The study described in this paper was a preliminary to fractography after fatigue tests of steel members with CFRP composites.

Acknowledgements

Financial support of these studies from Gdańsk University of Technology by the DEC-4/1/2023/IDUB/I3b/Ag grant under the ARGENTUM TRIGGERING RESEARCH GRANTS – ‘Excellence Initiative – Research University’ program is gratefully acknowledged.

REFERENCES

1. Yang, S.; He, Z.; Chai, J.; Meng, D.; Macek, W.; Branco, R.; Zhu, S.-P. A Novel Hybrid adaptive framework for support vector machine-based reliability analysis: A comparative study. *Structures* 2023, 58, 105665, <https://doi.org/10.1016/J.ISTRUC.2023.105665>
2. Kubit, A.; Macek, W.; Zielecki, W.; Szawara, P.; Myśliwiec, P. Experimental study of the impact of notches and holes made in the front edge of adherends on the properties of static and fatigue strength of adhesive joints. *Int J Adhes Adhes* 2024, 129, 103596, <https://doi.org/10.1016/J.IJADHADH.2023.103596>
3. Avanzini, A.; Donzella, G.; Gallina, D.; Pandini, S.; Petrogalli, C. Fatigue behavior and cyclic damage of peek short fiber reinforced composites. *Compos B Eng* 2013, 45, 397–406, <https://doi.org/10.1016/J.COMPOSITESB.2012.06.008>
4. Kowal, M.; Rozylo, P. Effect of bond end shape on CFRP/steel joint strength. *Compos Struct* 2022, 284, 115186, <https://doi.org/10.1016/J.COMPSTRUCT.2022.115186>
5. Mohabeddine, A.; Correia, J.; Montenegro, P.A.; De Jesus, A.; Castro, J.M.; Calçada, R.; Berto, F. An approach for predicting fatigue life of CFRP retrofitted metallic structural details. *Int J Fatigue* 2022, 154, 106557, <https://doi.org/10.1016/J.IJFATIGUE.2021.106557>
6. Duda, S.; Smolnicki, M.; Stabla, P.; Zielonka, P.; Osiecki, T.; Gao, C.; Lesiuk, G. Experimental characterization and modeling of cylindrical CFRP structures under quasi-static multiaxial loading conditions. *Thin-Walled Structures* 2024, 195, 111364, <https://doi.org/10.1016/J.TWS.2023.111364>
7. Macek, W. Post-failure fracture surface analysis of notched steel specimens after bending-torsion fatigue. *Eng Fail Anal* 2019, 105, 1154–1171, <https://doi.org/10.1016/J.ENGFAILANAL.2019.07.056>
8. Grochała, D.; Jasiewicz, M.; Filipowicz, K.; Parus, A.; Powalka, B.; Grzejda, R.; Zmarzły, P. Assessment of the functional properties of the surfaces of ductile cast iron parts. *Applied Sciences* 2024, 14, 9129, <https://doi.org/10.3390/APP14199129>
9. Macek, W.; Łagoda, T.; Mucha, N. Energy-based fatigue failure characteristics of materials under random bending loading in elastic-plastic range. *Fatigue Fract Eng Mater Struct* 2017, <https://doi.org/10.1111/ffe.12677>
10. Mecholsky, J.J. Fractography: Determining the sites of fracture initiation. *Dental Materials* 1995, [https://doi.org/10.1016/0109-5641\(95\)80045-X](https://doi.org/10.1016/0109-5641(95)80045-X)
11. Szala, M.; Szafran, M.; Matijošius, J.; Drozd, K. Abrasive wear mechanisms of S235JR, S355J2,

- C45, AISI 304, and Hardox 500 steels tested using garnet, corundum and carborundum abrasives. *Advances in Science and Technology. Research Journal* 2023, 17, 147–160, <https://doi.org/10.12913/22998624/161277>
12. Kwidzińska, D.B.; Jażdżewska, M.; Fydrych, D. The influence of selected metal oxides and laser modification on the surfaces of titanium alloys – bibliometric and systematic review. *Opt Laser Technol* 2025, 184, 112592, <https://doi.org/10.1016/J.OPTLASTEC.2025.112592>
13. Okuniewski, W.; Walczak, M.; Szala, M.; Chocyk, D. Effect of surface modification by shot peening on cavitation erosion resistance of titanium alloy Ti-6Al-4V produced by DMLS method. *Eng Fail Anal* 2025, 176, 109653, <https://doi.org/10.1016/J.ENGFAILANAL.2025.109653>
14. Chermant, J.L.; Coster, M. Quantitative fractography. *J Mater Sci* 1979.
15. Macek, W.; Branco, R.; Costa, J.D.; Pereira, C. Strain sequence effect on fatigue life and fracture surface topography of 7075-T651 aluminium alloy. *Mechanics of Materials* 2021, 160, 103972, <https://doi.org/10.1016/j.mechmat.2021.103972>
16. Pandian, K.T.; Neikter, M.; Bahbou, F.; Hansson, T.; Pederson, R. Elevated-temperature tensile properties of low-temperature HIP-treated EBM-built Ti-6Al-4V. *Materials* 2022, 15, 3624, <https://doi.org/10.3390/MA15103624>
17. Wang, Z.; Wu, W.; Qian, G.; Sun, L.; Li, X.; Correia, J.A.F.O. In-situ SEM investigation on fatigue behaviors of additive manufactured Al-Si10-Mg alloy at elevated temperature. *Eng Fract Mech* 2019, 214, 149–163, <https://doi.org/10.1016/J.ENGFRACMECH.2019.03.040>
18. Golewski, G.L. Comparative measurements of fracture toughness combined with visual analysis of cracks propagation using the DIC technique of concretes based on cement matrix with a highly diversified composition. *Theoretical and Applied Fracture Mechanics* 2022, 121, 103553, <https://doi.org/10.1016/J.TAFMEC.2022.103553>
19. Pojda, D.; Żarski, M.; Tomaka, A.A.; Luchowski, L. DpVision: Environment for multimodal images. *SoftwareX* 2025, 30, 102093, <https://doi.org/10.1016/J.SOFTX.2025.102093>
20. Macek, W.; Sampath, D.; Pejkowski, Ł.; Żak, K. A brief note on monotonic and fatigue fracture events investigation of thin-walled tubular austenitic steel specimens via fracture surface topography analysis (FRASTA). *Eng Fail Anal* 2022, 134, 106048, <https://doi.org/10.1016/J.ENGFAILANAL.2022.106048>
21. Kobayashi, T.; Shockey D. A fracture analysis via FRASTA, Part 2: Determining fracture mechanisms and parameters. *Advanced Materials & Processes* 1991, 140, 24–32.
22. Macek, W.; Tomczyk, A.; Branco, R.; Dobrzyński, M.; Seweryn, A. Fractographical quantitative analysis of EN-AW 2024 aluminum alloy after creep pre-strain and LCF loading. *Eng Fract Mech* 2023, 282, 109182, <https://doi.org/10.1016/J.ENGFRACMECH.2023.109182>
23. Zieliński, D.; Podulka, P.; Jiang, C.P.; Macek, W. Comparative assessment of entire bending-torsion fracture surface for 10HNP steel using different optical measurement techniques. *Advances in Science and Technology. Research Journal* 2025, 19, 267–274, <https://doi.org/10.12913/22998624/202668>
24. Macek, W.; Branco, R.; Podulka, P.; Masoudi Nejad, R.; Costa, J.D.; Ferreira, J.A.M.; Capela, C. The correlation of fractal dimension to fracture surface slope for fatigue crack initiation analysis under bending-torsion loading in high-strength steels. *Measurement* 2023, 218, 113169, <https://doi.org/10.1016/J.MEASUREMENT.2023.113169>
25. Charkaluk, E.; Bigerelle, M.; Iost, A. Fractals and fracture. *Eng Fract Mech* 1998, [https://doi.org/10.1016/S0013-7944\(98\)00035-6](https://doi.org/10.1016/S0013-7944(98)00035-6)
26. Macek, W.; Kopec, M.; Laska, A.; Kowalewski, Z.L. Entire fracture surface topography parameters for fatigue life assessment of 10H2M steel. *J Constr Steel Res* 2024, 221, 108890, <https://doi.org/10.1016/J.JCSR.2024.108890>
27. Krajewski, S.J.; Grochała, D.; Tomków, J.; Grzejda, R. Analysis of the surface stereometry of alloyed austenitic steel after fibre laser cutting using confocal microscopy. *Coatings* 2023, 13, 15 <https://doi.org/10.3390/COATINGS13010015>
28. Fahmy, A.; Gołębiewska, A.; Wojnicz, W.; Stanisławska, A.; Kowalski, J.; Łuczak, J.; Zaleska-Medynska, A.; Domínguez-Bella, S.; Martínez-López, J.; Molina-Piernas, E. Multi-functional monodispersed SiO₂-TiO₂ core-shell nanostructure and TEOS in the consolidation of archaeological lime mortars surfaces. *Journal of Building Engineering* 2023, 79, 107809, <https://doi.org/10.1016/J.JOBE.2023.107809>
29. Feng, G.; Jin, Z.; Jiang, Y.; Wang, X.; Zhu, D. Localized corrosion propagation of steel in cracked mortar and long-term corrosion of steel reinforcement in cracked concrete in seawater environment. *Corros Sci* 2024, 228, 111793, <https://doi.org/10.1016/J.CORSCI.2023.111793>
30. International Organisation of Standardization ISO 25178. Geometric Product Specifications (GPS) – Surface texture: areal 2010.
31. Macek, W.; Branco, R.; Szala, M.; Marciniak, Z.; Ulewicz, R.; Szczygiol, N.; Kardasz, P. Profile and areal surface parameters for fatigue fracture characterisation. *Materials* 2020, 13, 3691, <https://doi.org/10.3390/ma13173691>

32. Kubit, A.; Macek, W.; Zielecki, W.; Szawara, P.; Kłonica, M. fracture surface topography parameters for S235JR steel adhesive joints after fatigue shear testing. *Advances in Science and Technology Research Journal* 2023, 17, 130–139, <https://doi.org/10.12913/22998624/171490>
33. Wang, Y.; Meletis, E.I.; Huang, H. quantitative study of surface roughness evolution during low-cycle fatigue of 316L stainless steel using scanning white-light interferometric (SWLI) microscopy. *Int J Fatigue* 2013, 48, 280–288, <https://doi.org/10.1016/j.ijfatigue.2012.11.009>
34. Wynnyckyj, C.; Wise-Milestone, L.; Omelon, S.; Wang, Z.; Grynpas, M. Fracture surface analysis to understand the failure mechanisms of collagen degraded bone. *J Bone Miner Metab* 2011, 29, 359–368, <https://doi.org/10.1007/s00774-010-0233-9>
35. Carpinteri, A.; Spagnoli, A.; Vantadori, S. An approach to size effect in fatigue of metals using fractal theories. *Fatigue Fract Eng Mater Struct* 2002, 25, 619–627, <https://doi.org/10.1046/j.1460-2695.2002.00506.x>
36. Sampath, D.; Akid, R.; Morana, R. Estimation of crack initiation stress and local fracture toughness of Ni-Alloys 945X (UNS N09946) and 718 (UNS N07718) under hydrogen environment via fracture surface topography analysis. *Eng Fract Mech* 2018, 191, 324–343, <https://doi.org/10.1016/j.engfracmech.2017.12.010>
37. Franco, L.A.; Sinatora, A. 3D Surface Parameters (ISO 25178-2): Actual meaning of Spk and its relationship to Vmp. *Precis Eng* 2015, 40, 106–111, <https://doi.org/10.1016/j.precisioneng.2014.10.011>
38. Macek, W.; Sitek, R.; Podulka, P.; Lesiuk, G.; Zhu, S.P.; Liu, X.; Kopec, M. Fractography of Haynes 282 alloy manufactured by DMLS after Tensile and HCF. *J Constr Steel Res* 2025, 232, 109623, <https://doi.org/10.1016/J.JCSR.2025.109623>